Separation and Purification Technology 334 (2024) 126084

Contents lists available at ScienceDirect

Separation and Purification Technology

journal homepage: www.elsevier.com/locate/seppur

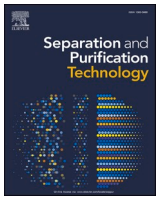

Valorization of acid mine drainage into potable water and valuable minerals through membrane distillation crystallization

Lebea N. Nthunya [a,c], Justine Pinier [b], Aamer Ali [a], Cejna Quist-Jensen [a,*], Heidi Richards [c,*]

[a] Center for Membrane Technology, Department of Chemistry and Bioscience, Aalborg University, Fredrik Bajers Vej 7H, 9220 Aalborg, Denmark
[b] Rennes University Institute of Technology, 3 Rue du Clos Courtel, 35000 Rennes, France
[c] Molecular Sciences Institute, School of Chemistry, University of the Witwatersrand, Private Bag X3, 2050 Johannesburg, South Africa

ARTICLE INFO

Keywords:
Membrane distillation crystallization
Resource recovery
Acid mine drainage
Mine tailings leachate
Circular economy

ABSTRACT

Owing to the rise in population growth and demands for the current living standards, mineral and water resources are depleting at the alarming rate. Also, the mineral–water-energy nexus raises a concern of high-quality water and mineral production at low costs. Membrane distillation crystallization (MDC) has emerged as a promising technology capable of simultaneous water and mineral recovery from wastewater or industrially discharged brines. Herein, the MDC was evaluated for recovery of water and precious minerals from acid mine drainage discharged from the mine tailings. High quality fresh water with 99.9 % salt rejection and permeate flux of 2.32 $kg{\cdot}m^{-2}{\cdot}h^{-1}$ was recovered at 52 °C feed inlet temperature. Also, feed temperatures were varied to determine their impact on mineral crystal morphology, size distribution and growth rate. Predominantly recovered minerals were gypsum, manganese fluoride, potassium iron oxide, nickel oxide hydroxide, sodium sulphate and dihydrogen sulphate. Orthorhombic crystal structure of mineral salts was attained at low feed inlet temperature (34 °C). Higher feed inlet temperatures (i.e. 41° C and 52° C) promoted co-crystallization giving rise to orthorhombic polymorph structures. Narrow crystal size distribution was reported at low water recovery factor (initial growth) for all temperatures. However, the particle size distribution broadened as the recovery factor increased. The crystal sizes ranged from 3.91 ± 0.97 μm to 14.04 ± 3.31. Remarkably, crystal growth rate increased with an increase in feed inlet temperature. These findings open a research direction towards economic recovery of mineral and water to supplement the existing shortages. With a myriad of crystals obtained from the MDC process, an additional operational unit is required to selectively recover high economic minerals.

1. Introduction

In the current era, world's demand for mineral resources increased significantly to meet their consumption due to improved living standards and global surge of rising technologies [1]. Due to mounting emphasis on renewable clean energy and use of electrical motor vehicles, the competition for mineral resources is significantly overwhelming the mining industry [2,3]. As a result, mining companies have expanded the search for commodities beyond terrestrial regions to meet the rising demands for minerals [4,5]. However, extraction of mineral resources from industrial wastewater could be used to supplement the existing shortages [6]. In doing so, discharge of high concentrated solutions will be minimized to protect the environment from pollution. In addition to mineral shortages, water scarcity and pollution has increased enormously because of population growth, climate change, industrial development polluting the existing freshwater resources [7,8]. For instance, mineral processing and hydrometallurgy generate aqueous streams constituting high concentrated minerals [9]. Also, during mining activities, sulphide minerals are disposed off in the mining tailings. Upon leaching from the tailings and reacting with oxygen, the sulphides generate acid mine drainage (AMD), thus considerably polluting the surface and ground water [10,11]. This problem is no exception in South Africa in regions dominated by mining activities [12]. Specifically, the AMD has become a South African legacy problem since inception of mining activities from the 20th Century. Since the closure of some mines in Johannesburg, the AMD was automatically decanting into the Western Basin, presenting an environmental catastrophe. Similarly, the closed mines in Johannesburg central and East Rand were filling up with a possible uncontrolled decantation into the environment. To develop sustainable treatment processes, innovative measures addressing these

* Corresponding authors.
E-mail addresses: Cejna@bio.aau.dk (C. Quist-Jensen), Heidi.richards@wits.ac.za (H. Richards).

https://doi.org/10.1016/j.seppur.2023.126084
Received 27 September 2023; Received in revised form 4 December 2023; Accepted 15 December 2023
Available online 16 December 2023

pressing issues are required.

Membrane processes have been widely evaluated for extraction of metals from ores and recovery of freshwater from concentrated solutions [13,14]. For instance, Fonseka et al (2022) evaluated nanofiltration/ adsorption hybrid systems for recovery of freshwater and rare earth elements (REE) from AMD [15]. The membrane process achieved high water fluxes (15.5 ± 0.2 $L{\cdot}m^{-2}{\cdot}h^{-1}$), salt rejections (98 %) while precious metal recovery (91 %) was achieved through adsorption processes [15]. Another study reported a comprehensive wastewater valorization towards recovery of copper minerals and freshwater, paying attention to emerging membrane technologies [16]. The waste valorization via selective membrane separation, membrane distillation crystallization (MDC) and reverse electrodialysis (RED) was a Chile case study due to high activities of copper mining. The reported findings presented remediation of wastewater into reusable clean water and copper mineral recovery, ensuring environmental protection and circular economy [16]. Also, treatment of reverse osmosis (RO) brines has attracted research interests due to strict disposal regulations affecting industry economics [17]. Similarly, mining of valuable mineral salts from the brines offers potential economic advantage. Though the extraction of brine dominating NaCl may not fall in line with economic feasibility, mining of elements such as Mg, Ca, Li, Br, B, and K are economically attractive [18,19]. To extract minerals from mine ores and RO concentrates, electrodialysis (ED), eutectic freeze crystallization (EFC), ion-exchange (IEX), and chemical processes have been widely used [20,21]. Extraction is achieved through thermodynamic alterations of the feed solutions. However, existing methods face economic and process challenges with no exception to fouling/scaling [22,23].

Currently, the MDC has emerged as a promising technology capable of extracting freshwater and minerals from high concentrated brines and wastewater discharged from industrial processes [24,25]. The MDC is a hybrid process involving membrane distillation integrated to a traditional crystallization, achieving controllable process performance [26]. Different from conventional crystallization processes, MDC controls rate of solution supersaturation, particle nucleation and growth [27,28]. Therefore, high purity particles of uniform size distributions are obtained. Also, high mineral extraction capacity with intensified process separation is achieved. Interestingly, intensification of the process is gearing towards efficient cleaner technology through utilization of solar energy [29].

Recovery of minerals in MDC is achieved through supersaturation of the feed solution while pure water passes through the membrane in vapour state [29,30]. Due to recovery of minerals from the feed, the MDC promotes zero-liquid discharge (ZLD), thus ensuring environmental protection and circular economy [22,30]. Although MDC has been successfully tested for recovery of various mineral salts including sodium chloride, magnesium/ calcium salts, its evaluation towards extraction of precious minerals from the mine tailing leachates and/or AMD is rarely reported. In our previous study, the laboratory-scale prepared polyvinylidene fluoride (PVDF) flat sheet membranes were evaluated towards resource recovery via MDC [31]. The flat sheet membranes presented various challenges including fouling, flux decay and non-uniform size distribution of produced crystals. The current study focused on treatment of AMD leaching from the mine tailings into Fleurhof dam (Johannesburg, South Africa). Similarly, the mineral recovery from AMD using hollow fibre direct contact membrane distillation crystallization (HF-DCMDC) is reported for the first time.

2. Experimental procedure

2.1. Materials

The salts used to prepare the synthetic feed solutions were purchased from Sigma Adrich (Germany). These salts include aluminium nitrate ($Al(NO_3)_3$), sodium chloride (NaCl), calcium nitrate ($Ca(NO_3)_2$), cobalt chloride ($CoCl_2$), sodium nitrate ($NaNO_3$), zinc sulphate ($ZnSO_4$), iron sulphate ($FeSO_4$), magnesium sulphate ($MgSO_4$), potassium sulphate (K_2SO_4), nickel sulphate ($NiSO_4$), manganese sulphate ($MnSO_4$), and sodium fluoride (NaF). All chemicals were used as received. A commercial polypropylene (PP) module consisting of 40 hollow fibre membranes (length of 50 cm and surface area of 0.1 m^2) was purchased from Microdyn-Nadir (MD020CP2N). The membrane has overall porosity of 73 %, average pore size of 0.2 μm and thickness of 450 μm. De-ionized water was prepared from our lab using Direct-Q® (Millipore) system supplied by Merck Millipore (Denmark).

2.2. Membrane crystallization tests

Synthetic feed solution was prepared to mimic characteristics of AMD water samples from mine tailings leachates discharged to Fleuhorf Dam (South Africa). Table 1 presents mineral concentrations of synthetic solutions used in the current study. To minimize duration of crystal formation, the concentration was increased by a factor of 10 prior to MDC.

Test experiments were carried out in a crossflow HF-DCMDC set-up. A synthetic AMD feed solution (2 L) was transferred into Schott Duran bottle (feed tank)-equipped with a lid. The HF-DCMDC connected to the feed and permeate tanks was run continuously until supersaturation of the feed (Fig. 1). The system was operated using a countercurrent configuration with crossflow velocity of 14.03 mL/sec for both feed and permeate sides driven by a peristaltic pump (MasterFlex L/S). The crossflow velocity was chosen on the basis of the reported literature [32,33]. The temperature sensors were installed at the module inlet and outlet of the feed and permeate. Three feed inlet temperatures were evaluated to understand their impact on crystal formation. The measured feed inlet temperatures were 35 °C, 41 °C, and 52 °C while the feed outlet temperatures were 32 °C, 38 °C, and 36 °C. The measured permeate inlet temperatures were 18 °C, 20 °C, and 29 °C while the permeate outlet temperatures were 21 °C, 27 °C, and 33 °C. These inlet and outlet temperatures were used to calculate average temperature difference across the membrane interface following Eqs. (1)–(3). The water flux and salt rejection were calculated by measuring the weight increase and conductivity of the permeate using balance (KERN EMS) and conductivity meter (Mettler Toledo, F30-Standard) respectively. Eqs. (4) and (5) were used to calculate the permeated flux and salt rejection respectively. The MDC process flow diagram is presented in Fig. 1. The supersaturated retentate was transferred into a jacketed crystallization reactor (Glass Chem crystallizer-equipped with BLDC stirring motor) for separation of crystals and water residue. The crystallization reactor was used to filter the excess water from the crystals under constant mechanical stirring. To minimize membrane fouling, a physical cleaning of the MDC system was carried out at the end of each test feed temperature using deionized water. The water cross velocity was circulated at rate higher than the MDC operating flow rate to ensure removal of salts deposit on the surface of the membrane. The cleaning

Table 1
Composition of salts used in the study and their corresponding concentrations.

Salts	Concentrations (mg/L)	10× concentrated (mg/L)
NaCl	4.84	48.40
$NaNO_3$	4.63	46.30
$MgSO_4$	4.32	43.20
K_2SO_4	1.36	13.60
$Ca(NO_3)_2$	0.86	8.60
$Al(NO_3)_3$	0.37	3.70
$MnSO_4$	0.37	3.70
$FeSO_4$	0.10	1.00
$CoCl_2$	8.47×10^{-7}	8.47×10^{-6}
NaF	2.62×10^{-7}	2.62×10^{-6}
$ZnSO_4$	7.74×10^{-8}	7.74×10^{-7}
$NiSO_4$	8.40×10^{-8}	8.40×10^{-7}
pH	4.80	5.20
H^+	$1.00 \times 10^{-4.8}$	$1.00 \times 10^{-5.2}$

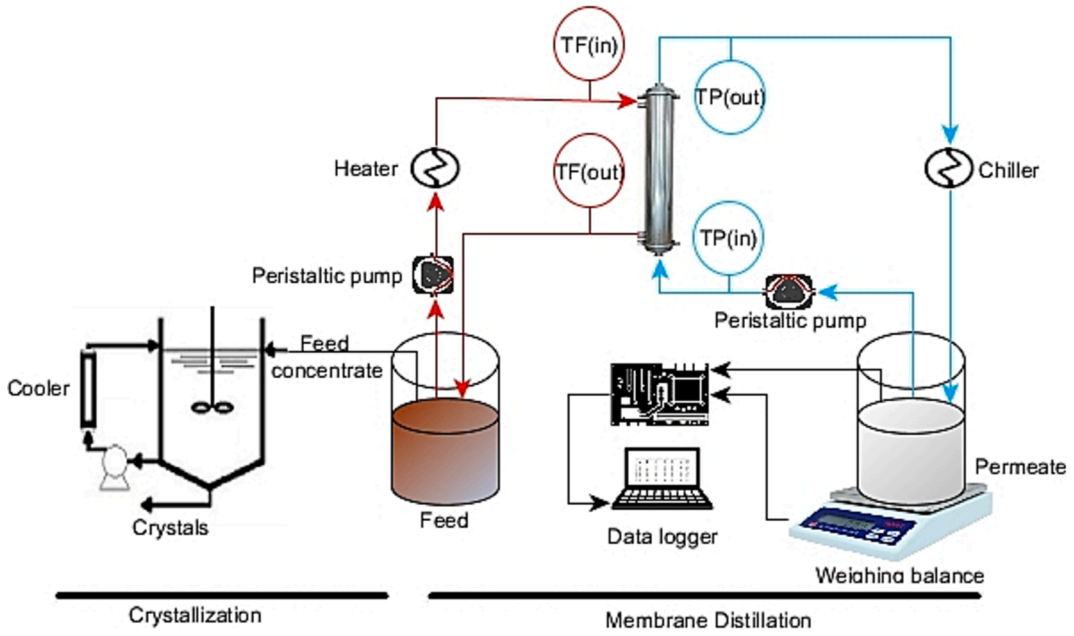

Fig. 1. Schematic illustration of the MDC systems used for recovery of freshwater and mineral salts. The $T_{F(in)}$, $T_{F(out)}$, $T_{P(in)}$, and $T_{P(out)}$ represent feed inlet and outlet temperatures and permeate inlet and outlet temperatures respectively.

process was carried out for 60 min.

$$\Delta T_{ln} = \frac{\Delta T_{in} - \Delta T_{out}}{In \frac{\Delta T_{in}}{\Delta T_{out}}} \quad (1)$$

$$\Delta T_{in} = T_{feed,in} - T_{permeate,out} \quad (2)$$

$$\Delta T_{out} = T_{feed,out} - T_{permeate,in} \quad (3)$$

$$J = \frac{dm}{Adt} \quad (4)$$

$$R(\%) = \frac{k_f - k_p}{k_f} x100\% \quad (5)$$

where $J, R(\%), dm, A, dt, k_f$ and k_p represent water flux, percentage salt rejection, mass difference at time (t), membrane active surface area, change in time, feed and permeate conductivity respectively.

2.3. Crystal characterization

Crystal nucleation and growth were monitored using an optical microscope (Zeiss Axiolab 5 equipped with an Axiocam 208 color). To analyze the crystal formation and growth, 1 mL of the feed solution was collected from the feed tank upon saturation and preserved in a warm bath while carried to the optical microscope analysis. The crystal containing solution was spread on a glass-plate and crystal images were captured. The crystal-containing solution was sampled after every 20 min from the feed tank. An open-source software, namely ImageJ was used to measure the size of crystals. To ensure a true reflection of particle size distribution, a minimum of 100 crystals were analyzed. The crystal particle growth rate was calculated from a linearized plot of particle size as a function of time [34]. The approach considered the effective growth rate as the time derivative of the crystal size. Eq. (6) was used to evaluate the crystal growth rate (G^{eff}). The G^{eff} was estimated from the slope of the linearized plot following Eq. (7) [34].

$$G^{eff} = \frac{1}{2}\frac{dL}{dt} \quad (6)$$

$$dL = 2G^{eff} dt \quad (7)$$

where dL, dt, and G^{eff} were change in crystal length, growth time and effective growth rate. Constant factor ($\frac{1}{2}$) accounts for particle growth from crystal centre to two opposite directions.

Geochemical software PHREEQC (interactive-version 3.7.3) was used to simulate salts precipitation from the AMD utilizing the thermodynamic database ANDRA/RWM – THERMOCHIMIE-TDB (www.thermochimie-tdb.com). The concentration of the feed solution (Table 1) was used as input parameters for PHREEQC, along with other specifications including temperatures (34, 41, 52 °C), recovery factors range of 0–80 % and pH 5. The pH value was fixed at 5 throughout all the simulations. To ascertain the simulation and formation of crystal structure, XRD analysis was carried out using powder x-ray diffraction (PXRD, Bruker D2 Phaser Diffractometer equipped with a non-monochromated Co-Kα source, λ = 1.785 Á).

3. Results and discussion

3.1. Effect of feed temperature on water flux and salt rejection

Obtained water flux was used to evaluate the performance of MDC at different operating temperature (Fig. 2). The pure water and mineralized water permeability is presented in Fig. 2a and b. The flux of pure and mineralized water increased upon increase in feed temperature. Fig. 2c shows a large deltaT at high feed temperature thus indicating the high driving force. DeltaT representing MD process driving force remained relatively constant with minimal variations. Initial deltaT at t_0 were 13.6, 16.3 and 17.7 at 34 °C, 41 °C, and 52 °C respectively. The final deltaT decreased slightly at 34 °C, 41 °C, markedly dropping to 13.1 and 15.1 respectively. These variations presented possible occurrence of temperature polarization (TP). The TP was induced by differences in feed temperature at the hollow fibre membrane to the temperature of the bulk feed. However, 52 °C presented high resistance to TP, technically due to improved temperature distribution between the feed at the membrane interface and the bulk solution. The pure water flux remained relatively stable for all temperatures. At the beginning of the MDC process, the permeate flux of the pure water was lower than that of the synthetic AMD. This discrepancy was associated with the heat transfer through the membrane causing the temperature reduction in the feed stream and increase in distillate temperature. According to

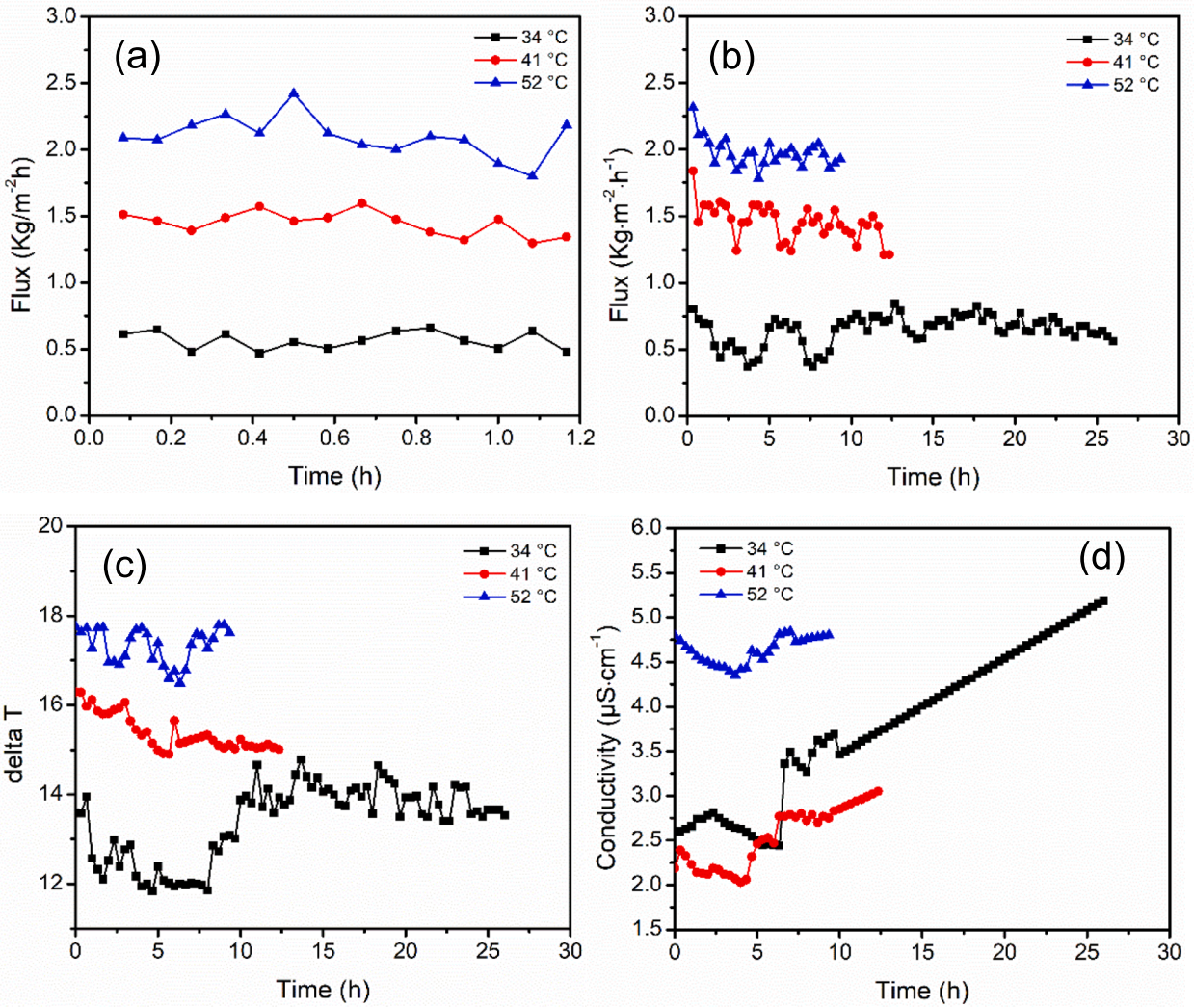

Fig. 2. Evaluation of MDC process performance: (a) pure water flux, (b) mineralized water flux (c) temperature gradient (d) and permeate conductivity as a function of time.

Gryta (2012), the heat transfer through the membrane is associated with the heat conduction and latent heat influenced by the vapour flowing through the membrane [35]. The specific heat capacity and/or the heat transfer coefficient of fresh water is higher than that of salty water [36]. As a result, the latent heat transfer is faster in pure compared to mineralized AMD, thus lowering the temperature difference across the membrane leading to lower flux. Compared to pure water, the flux of the AMD presented minimal variation with some degree of resistance to change. The resistance of MD flux variation corresponds to low wetting character of the membranes [37,38]. This property is key towards high salt rejection. The flux of mineralized water increased from 0.80 $L{\cdot}m^{-2}{\cdot}h^{-1}$, to 1.84 $L{\cdot}m^{-2}{\cdot}h^{-1}$ upon an increase in feed inlet temperatures from 34 °C to 41 °C. Similarly, the flux Increased to 2.32 $kg{\cdot}m^{-2}{\cdot}h^{-1}$ at 52 °C. Water fluxes presented resistance to flux decay with minimal decline until salts saturation and crystallization. Slight decrease in permeate flux was attributed to accumulation of mineral salts on the surface of the membrane, obstructing the movement of the water vapour through the membrane pores (A process known as concentration polarization). Additionally, increasing the concentration of salts in the feed solution reduced the vapour pressure of the retentate. Dissolved salts reduce the water activity, thus lowering the free energy of the water molecules. Technically, the mineral salts form hydrogen bonds with the water molecules, thus requiring additional energy to convert water into vapour [39]. Similar findings where increase in salt concentration reduced the permeate flux in DCMD has been reported in various studies [40–42]. Upon use of similar volume of feed solution, the MD process reached highest water recovery at different time interval. For instance, the highest water recovery of 2 L feed solution was attained after 26 h, 12.3 h and 9.3 h at feed inlet temperatures of 34 °C, 41 °C and 52 °C respectively. The advantage of MDC over other desalination technologies is the process resistance towards concentration polarization (CP) [43]. The permeate conductivity increased consistently upon saturation of feed solution (Fig. 2d). However, the increase was minimal indicating membrane resistance to wetting. The reported conductivity corresponds to salts rejection >99.9 %.

3.2. *Change in distillate flux as a function of recovery factor*

The water flux and deltaT reported as a function of recovery factor at various thermal conditions is presented in Fig. 3. DeltaT and flux remained relatively stable with minimal decline caused by TP along the module length. Similarly, low feed temperatures (technically at 34 °C) presented significant deltaT and flux fluctuations. This was attributed to poor heat distributions between the feed at the membrane interface and the bulk of the feed. High flux fluctuations were reported at low water recovery factors <40 %. At low recovery factors, the distribution of the bulk temperature was inhomogeneous causing profound impact on flux stability. Intense fluctuations were seen from deltaT of the lower feed

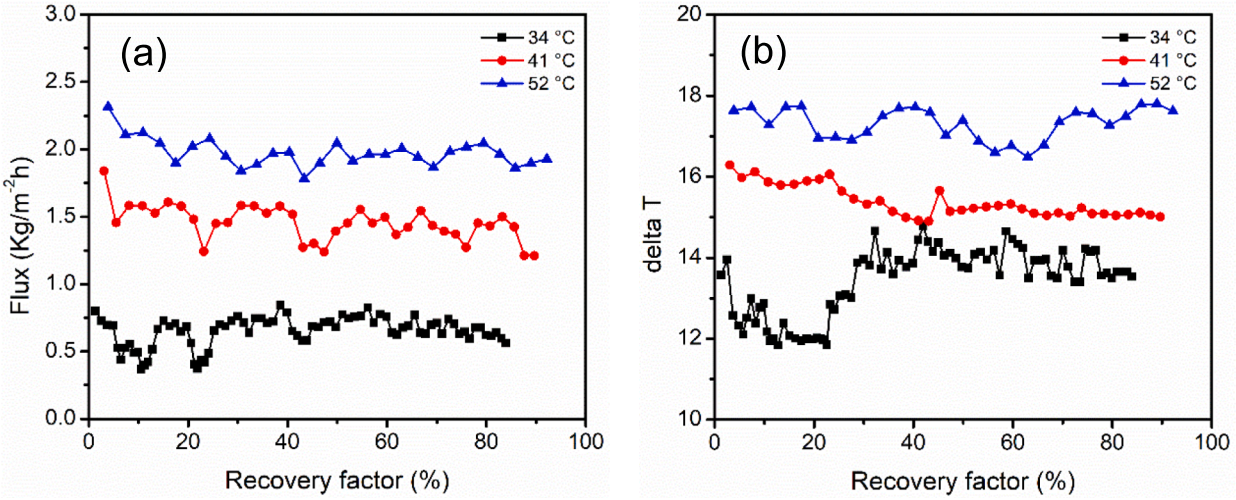

Fig. 3. Water flux (a) and change in temperature across the membrane for three feed temperatures (b) as a function of recovery factor.

inlet temperature. Although deltaT remained relatively constant as a function of recovery factor, the permeate flux decreased slightly. For instance, initial flux was 0.8 $L{\cdot}m^{-2}{\cdot}h^{-1}$, 1.8 $L{\cdot}m^{-2}{\cdot}h^{-1}$, and 2.3 $L{\cdot}m^{-2}{\cdot}h^{-1}$, at 1 % recovery factor for 34 °C, 41 °C and 52 °C feed inlet temperatures respectively. The highest recovery factors translated to a flux decrease, affording 0.7 $L{\cdot}m^{-2}{\cdot}h^{-1}$, 1.2 $L{\cdot}m^{-2}{\cdot}h^{-1}$, and 1.9 $L{\cdot}m^{-2}{\cdot}h^{-1}$, at feed temperatures of 34 °C, 41 °C and 52 °C respectively. Recovery factors at these feed inlet temperatures were 83.4 %, 89.6 % and 92.2 %. The decrease in permeate flux was attributed to vapour pressure drop caused by concentration of the salts accumulating near the membrane interface [44]. Technically, solute aggregates of the concentrated feed deposited on membrane pores, causing flux decline. According to Ali et al, (2015), the increase in solute concentration decreases the MD driving force due to suppression of the vapour pressure [25]. Based on the recovery factors, 83.4 %, 89.6 % and 92.2 % of the total feed solutions were recovered as per feed inlet temperatures (34, 41 and 52 °C) respectively. The unrecovered feed was influenced by the dead volume remaining in the process connections including the tubing and module.

3.3. PHREEQC solubility simulations and XRD analysis of the recovered mineral salts

The PHREEQC solubility simulations and XRD analysis were carried out to understand the crystal formation and crystallography of the recovered mineral salts and results are presented in Fig. 4. Abundant recovered salts included gypsum ($CaSO_2{\cdot}2H_2$) as designated by the JCPDS card values for planes (0 2 0), (0 2 1), and (0 4 1) at $2\theta = 11.58°$, 20.72°, and 29.11° respectively. Based on the PHREEQC solubility simulations, 10.3 kg of gypsum precipitated from 1 m^3 of the feed solution at RF = 80 %. Also, JCPDS card values for planes (1 1 0) and (2 1 1) at respective $2\theta = 23.41°$ and 50.27° corresponded to the characteristics diffractions peaks of manganese fluoride (MnF_2) while (2 0 0) and (1 1 2) at respective $2\theta = 31.82°$ and 40.75° corresponded to diffractions peaks of potassium iron oxide ($KFeO_2$) and aluminium oxide hydroxide (AlO(OH)). Other traces of mineral salts were sodium sulphate ($N_2S_2O_6$), cobalt chloride hydrate ($CoCl_2{\cdot}2H_2$), and dihydrogen sulphate ($H_2S_2O_7$). The trace precipitation of these compounds was justified by PHREEQC solubility simulations at RF = 80 %. These include aluminium and iron compounds at high trace levels and cobalt, nickel, aluminium, and low trace levels. During saturation and precipitation, some salts underwent

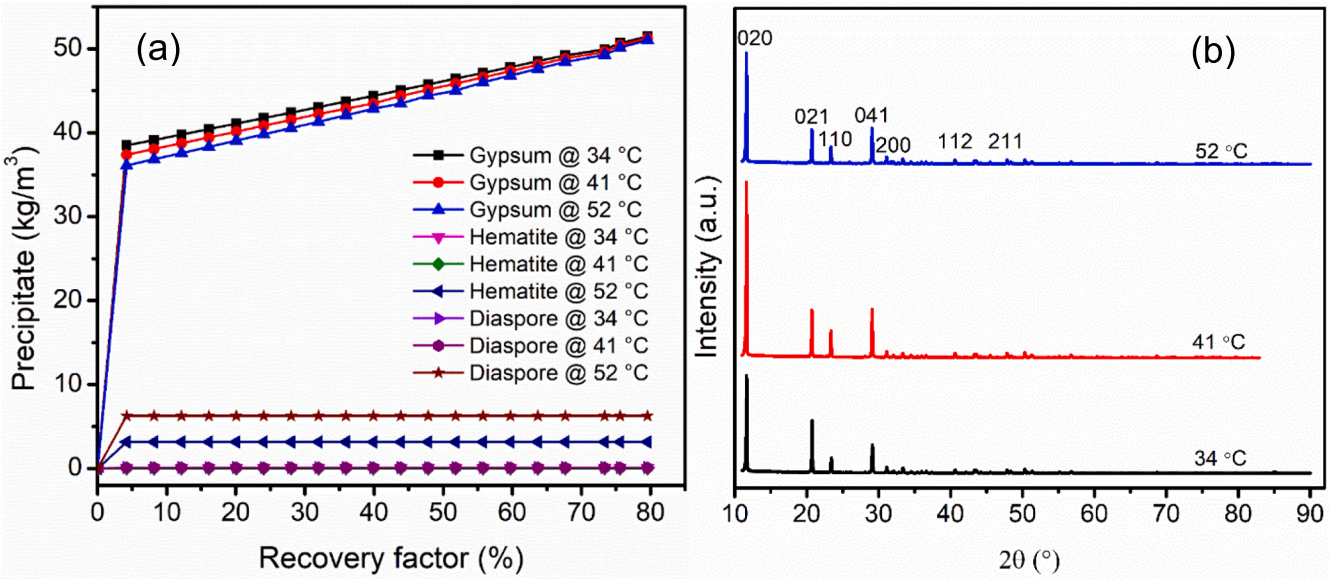

Fig. 4. Mineral salts at various feed temperatures; (a) The PHREEQC solubility simulations and (b) XRD patterns.

metathesis reactions. These was seen as certain ionic compounds such as $MnSO_4$, and NaF exchanged ions formed MnF_2 and $N_2S_2O_6$. The formation of the salt's replacement reaction was similar for all different feed temperatures. The Crystallographic information presented the dominant formation of monoclinic crystal structures of gypsum with a C2/c space group. Nonetheless, trace compounds presented varying crystal structures. For instance orthorhombic $KFeO_2$ and AlO(OH), tetragonal MnF_2 and monoclinic $CoCl_2{\cdot}2H_2$. The crystallographic parameters supported the morphological structure of the crystal salts presented in the microscopy analysis.

3.4. Morphology of crystal structures

The AMD is characterized by a wide composition of different mineral salts. These salts crystallize in various forms of hydration and crystal structures [45]. In MDC, crystal formation and growth are influenced by rate of supersaturation. Salts are saturated upon exceeding their solubility in water. Also, salts solubility is affected by process temperature. Owing to their differences in water solubility, different salts crystallize at different concentrations in solution [46]. In the current study, crystal formation and growth were monitored using an optical microscope. The crystals were formed through the arrangement of ions, atoms, or molecules in a characteristic pattern of a crystal structure, a process known as nucleation. These small crystals form a suitable site for additional deposition of other ions or atoms, a process known as crystal growth [47]. Prior to nucleation, ions/atoms required the seeding sites to form the nuclei. To some extent, Mullin (2001) defined a possible nucleation taking place in the absence of the crystalline matter, giving rise to primary nucleation [48]. In MDC, the membrane acted as an interface promoting nucleation upon supersaturation of the mineral salts [28]. Technically, sparingly soluble salts formed the nuclei and grew into crystal, thus acting as sites for growth of large crystals. At initial growth stage, single orthorhombic crystal structure was seen at lower feed inlet temperature (i.e. 34 °C). Similarly, co-crystallization took place at higher feed inlet temperatures (i.e. 41 and 52 °C) giving rise to orthorhombic polymorph structures. High temperatures induced fast crystal growth rate (Fig. 5d) giving rise to co-crystallization. During growth propagation, minerals were dominated by monoclinic crystal structure at low feed temperature (i.e. 34 and 41 °C). However, mixed monoclinic and orthorhombic crystal structure were recorded at high feed inlet temperature (i.e. 52 °C). At low temperatures, the crystals lost orthorhombic structures at a faster rate, forming monoclinic crystal structure [49]. Upon temperature alteration, the mineral salts underwent magnetic phase transition giving rise to mixed crystal structures at 52 °C. However, further saturation of the feed solution at higher recovery factors transformed orthorhombic structures to monoclinic structures with different patterns of particle growth.

3.5. Effect of feed temperature on particle size distribution and growth rate

Similar to other crystallization techniques, the MDC produces crystal particles of different sizes depending on growth conditions. Based on the specific mode of application, evaluation of crystal size distribution is key. This is because the size distribution has an impact on the product properties and processing requirements [50]. For instance, crystal of different sizes and shape are characterized by different rates of dissolution in solution [51,52]. In this study, the crystal size distribution was evaluated through analysis of microscopic images. The crystal particle distribution was acquired from non-linear Lorentz model and presented in Fig. 6. Narrow crystal size distribution was reported at low water recovery factors (initial growth) for all feed temperatures. Specific range of crystal size was 3.91 ± 0.97–6.01 ± 1.59 μm at 32–37 % recovery factor (Table 2). The narrow size distribution was linked to the formation of similar types of mineral crystals. For instance, minerals of low solubility form uniform crystal structures at low RF. However, the particle size distribution broadened as the recovery factor increased. Specific crystal sizes ranged from 10.59 ± 4.01 to 16.86 ± 5.89 at 42 %–63 % recovery factors (Table 2). Notably, crystal structure is constrained by internal geometry of the particles. However, in addition to external temperature, crystal structure and growth rate were affected by presence of impurities. For instance, the AMD is characterized by concoction of different mineral salts. Some mineral salts acted as an impurity to the other, thus affecting the crystal growth rate [53]. During growth patterns, the mineral salts were bound to each other, thus altering the crystal faces. These alterations to growth patterns broadened the

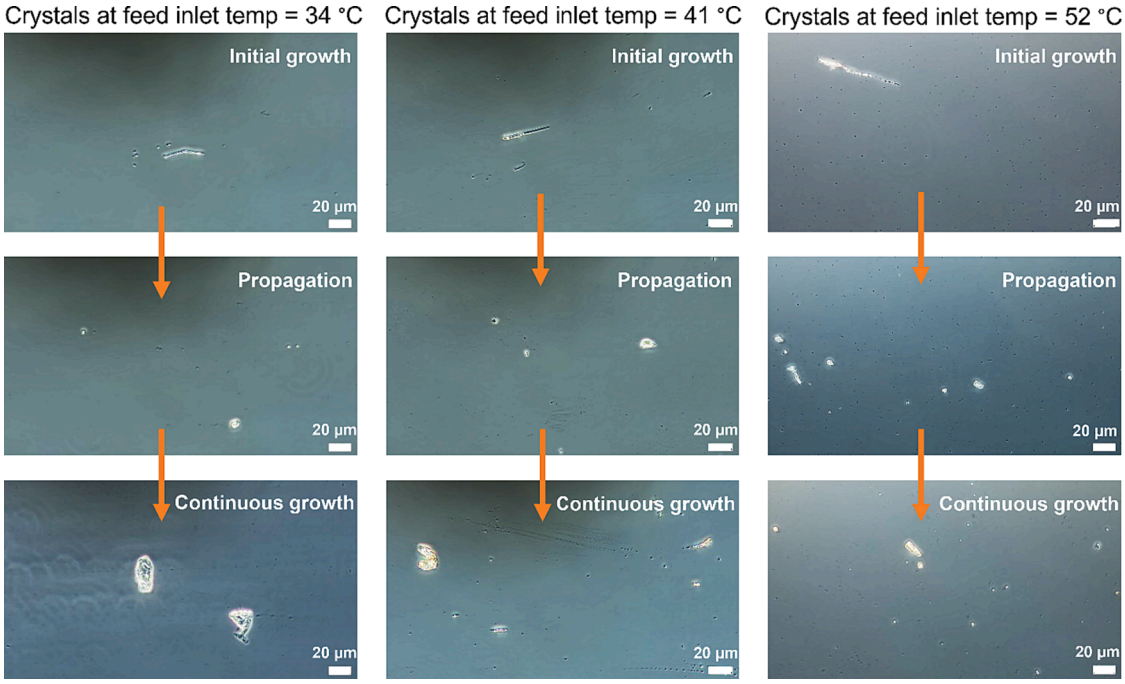

Fig. 5. Microscopic images of the recovered minerals salts at 34 °C, 41 °C, and 52 °C feed temperatures.

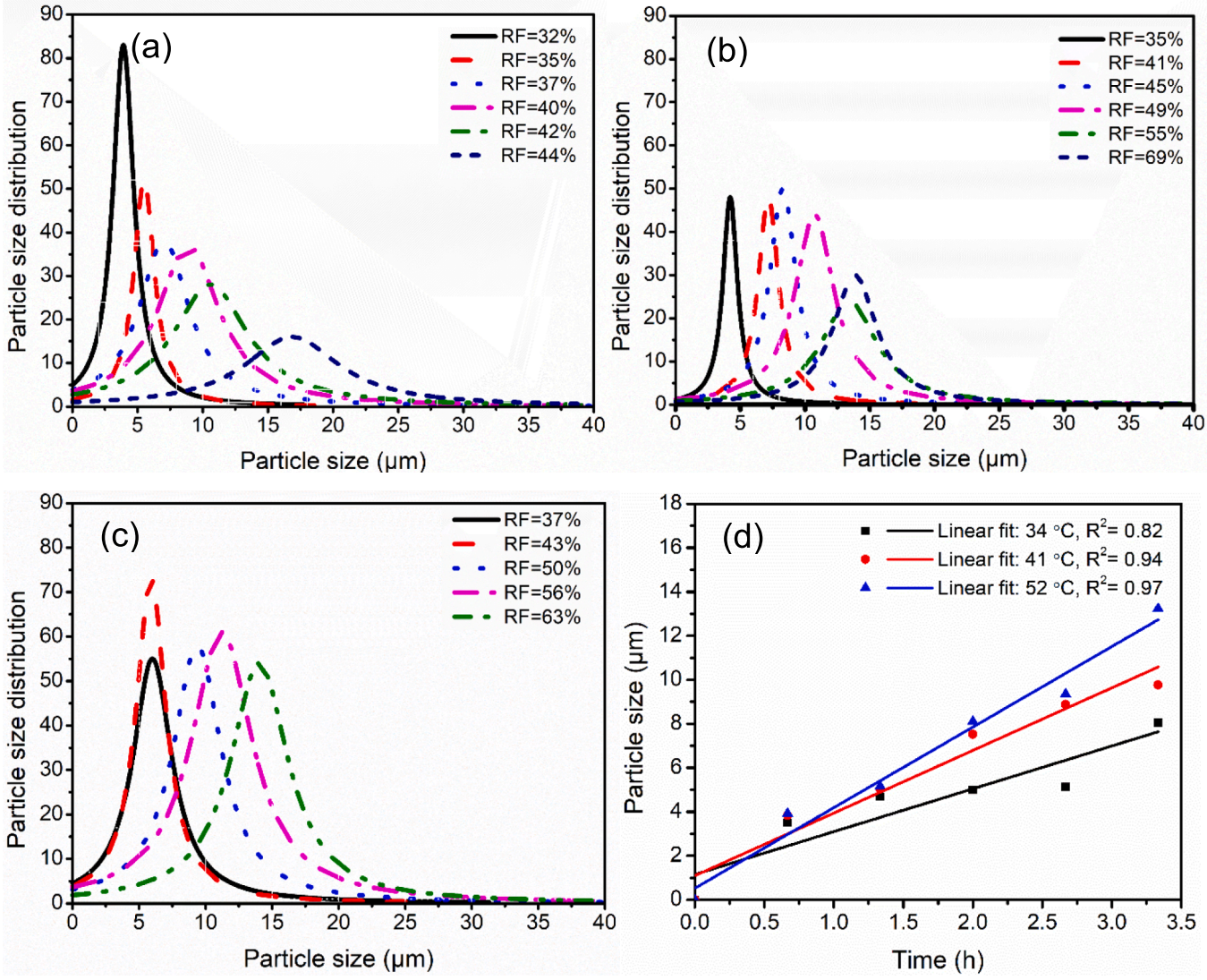

Fig. 6. Size distribution of particle growth at different feed temperatures (a) 34 °C, (b) 41 °C, (c) 52 °C, (d) linearized particle growth rate as function of time.

Table 2
Effect of feed temperature (34 °C, 41 °C, and 52 °C) on particle size growth at different recovery factors.

Feed temperature					
34 °C		41 °C		52 °C	
Recovery Factor (%)	Particle size (μm)	Recovery factor (%)	Particle size (μm)	Recovery factor	Particle size (μm)
32	3.91 ± 0.97	35	4.22 ± 1.37	37	6.01 ± 1.59
35	5.51 ± 0.94	41	7.17 ± 1.94	43	5.90 ± 0.76
37	7.03 ± 2.39	45	8.29 ± 2.52	50	9.37 ± 2.45
40	8.91 ± 3.78	49	10.74 ± 3.70	56	11.21 ± 3.65
42	10.59 ± 4.01	55	13.40 ± 4.25	63	14.04 ± 3.31
44	16.86 ± 5.89	69	13.85 ± 4.10	–	–

distribution of particle sizes. However, broadening of size distribution was reduced as the feed temperature increased. This was associated with the high rate of crystal growth at high temperatures. For instance, the crystal growth rate was 0.95 ± 0.20 μm·h^{-1} at 34 °C. This increased to 1.42 ± 0.16 μm·h^{-1} and 1.83 ± 0.14 μm·h^{-1} at 41 °C and 52 °C respectively (Table 3). The increase in temperature increased the rate of water recovery, thus increasing rate of supersaturation. As a result, the crystal growth rate increased.

4. Conclusion

Herein, the MDC was evaluated towards simultaneous extraction of precious minerals and high purity water from the AMD (water leachate from mine tailings). Complementary water fluxes, specifically 2.3 L·m^{-2}·h^{-1}, and 99.9 % salt rejection were attained at the highest feed inlet temperature (52.4 °C). The MDC produced various salts ($CaSO_2{\cdot}2H_2$, MnF_2, $KFeO_2$, NiO(OH), $N_2S_2O_6$, $CoCl_2{\cdot}2H_2$, and $H_2S_2O_7$) with different sizes and crystal structures at different growth conditions. At early stage of crystal growth, orthorhombic crystal structures were recorded with sizes 3.91 ± 0.97 μm, 4.22 ± 1.37 μm and 6.01 ± 1.59 μm

Table 3
Crystal growth rate at different feed temperatures.

Temperature (°C)	Crystal growth rate (μm·h^{-1})	R^2
34	0.95 ± 0.20	0.82
41	1.42 ± 0.16	0.94
52	1.83 ± 0.14	0.97

at 34.6 °C, 41.5. °C and 52.4 °C feed inlet temperatures respectively. Similarly, narrow crystal size distribution was recorded at early growth stage. The crystal structures changed to monoclinic as the water recovery increased. Crystal size distribution broadened at higher water recovery. Specifically, the crystal sizes ranged from 10.59 ± 4.01 to 16.86 ± 5.89 at 42–63 % recovery factors. The mineral salts co-crystalized at higher feed inlet temperature 41.5 °C and 52.4 °C giving rise to orthorhombic polymorph structures. Although size distribution broadened at higher recovery factors, this was reduced as the feed inlet temperature was increased. This reduction was linked to an increased rate of crystal growth. For instance, crystal growth rates were 0.95 ± 0.20 μm·h^{-1}, 1.42 ± 0.16 μm·h^{-1}and 1.83 ± 0.14 μm·h^{-1} at 34 °C, 41 °C and 52 °C respectively. However, further saturation of the feed solution at higher recovery factors transformed orthorhombic structures to monoclinic structures with different patterns. This was evidenced by crystallography parameters of the obtained crystal presenting monoclinic crystal structures of $CaSO_2{\cdot}2H_2$ and $CoCl_2{\cdot}2H_2$. However, orthorhombic $KFeO_2$ and AlO(OH), tetragonal MnF_2 were recorded, though their morphology was not recorded from the microscope due to their precipitation in trace amounts. These reported findings will open research directions towards improved MDC process performance and ultimately pilot scale evaluation.

5. Author statement

During the preparation of this work the authors used OriginPro and ImageJ softwares in order to process the data. After using this softwares, the authors reviewed and edited the content as needed and take full responsibility for the content of the publication. Also, authors declare that the manuscript was prepared without the use of AI-assisted technologies. The authors wrote the manuscript by virtue of utilizing the existing literature to support our statement.

CRediT authorship contribution statement

Lebea N. Nthunya: Conceptualization, Methodology, Software, Validation, Formal analysis, Investigation, Data curation, Writing – original draft, Writing – review & editing, Visualization. **Justine Pinier:** Investigation, Methodology, Writing – original draft. **Aamer Ali:** Data curation, Formal analysis, Software. **Cejna Quist-Jensen:** Conceptualization, Data curation, Funding acquisition, Project administration, Resources, Supervision, Validation. **Heidi Richards:** Conceptualization, Funding acquisition, Project administration, Resources, Supervision, Validation, Visualization.

Declaration of competing interest

The authors declare that they have no known competing financial interests or personal relationships that could have appeared to influence the work reported in this paper.

Data availability

Data will be made available on request.

Acknowledgements

This research was funded by the Ministry of Foreign Affairs of Denmark (MFA) through the Danida Fellowship Centre (DFC), project no. 20-M01AAU, “Membrane crystallization for water and mineral recovery”. The study was conducted at Aalborg University (Denmark) and the University of the Witwatersrand (South Africa). Support from the MFA and these universities is highly acknowledged.

References

[1] J.J. Siirola, Speculations on global energy demand and supply going forward, Curr. Opin. Chem. Eng. 5 (2014) 96–100, https://doi.org/10.1016/j.coche.2014.07.002.
[2] N. Dushyantha, N. Batapola, I.M.S.K. Ilankoon, S. Rohitha, R. Premasiri, B. Abeysinghe, N. Ratnayake, K. Dissanayake, The story of rare earth elements (REEs): Occurrences, global distribution, genesis, geology, mineralogy and global production, Ore Geol. Rev. 122 (2020), 103521, https://doi.org/10.1016/j.oregeorev.2020.103521.
[3] B.C. McLellan, G.D. Corder, D.P. Giurco, K.N. Ishihara, Renewable energy in the minerals industry: A review of global potential, J. Clean. Prod. 32 (2012) 32–44, https://doi.org/10.1016/j.jclepro.2012.03.016.
[4] T. Prior, D. Giurco, G. Mudd, L. Mason, J. Behrisch, Resource depletion, peak minerals and the implications for sustainable resource management, Glob. Environ. Chang. 22 (2012) 577–587, https://doi.org/10.1016/j.gloenvcha.2011.08.009.
[5] O. Sparenberg, A historical perspective on deep-sea mining for manganese nodules, 1965–2019, Extr. Ind. Soc. 6 (2019) 842–854, https://doi.org/10.1016/j.exis.2019.04.001.
[6] M. Schmidt, Scarcity and environmental impact of mineral resources-an old and never-ending discussion, Resources 8 (2019) 1–12, https://doi.org/10.3390/resources8010002.
[7] Y. Bettini, R. Brown, F.J. De Haan, Water scarcity and institutional change: Lessons in adaptive governance from the drought experience of Perth, Western Australia, Water Sci. Technol. 67 (2013) 2160–2168, https://doi.org/10.2166/wst.2013.127.
[8] F.R. Rijsberman, Water scarcity: Fact or fiction? Agric. Water Manag. 80 (2006) 5–22, https://doi.org/10.1016/j.agwat.2005.07.001.
[9] F. Xie, T.A. Zhang, D. Dreisinger, F. Doyle, A critical review on solvent extraction of rare earths from aqueous solutions, Miner. Eng. 56 (2014) 10–28, https://doi.org/10.1016/j.mineng.2013.10.021.
[10] I. Park, C.B. Tabelin, S. Jeon, X. Li, K. Seno, M. Ito, N. Hiroyoshi, A review of recent strategies for acid mine drainage prevention and mine tailings recycling, Chemosphere 219 (2019) 588–606, https://doi.org/10.1016/j.chemosphere.2018.11.053.
[11] J.G. Skousen, P.F. Ziemkiewicz, L.M. McDonald, Acid mine drainage formation, control and treatment: Approaches and strategies, Extr. Ind. Soc. 6 (2019) 241–249, https://doi.org/10.1016/j.exis.2018.09.008.
[12] T.S. McCarthy, The impact of acid mine drainage in South Africa, S. Afr. J. Sci. 107 (2011) 1–7, https://doi.org/10.4102/sajs.v107i5/6.712.
[13] H. Koseoglu, M. Kitis, The recovery of silver from mining wastewaters using hybrid cyanidation and high-pressure membrane process, Miner. Eng. 22 (2009) 440–444, https://doi.org/10.1016/j.mineng.2008.11.006.
[14] C.A. Quist-Jensen, A. Ali, S. Mondal, F. Macedonio, E. Drioli, A study of membrane distillation and crystallization for lithium recovery from high-concentrated aqueous solutions, J. Memb. Sci. 505 (2016) 167–173, https://doi.org/10.1016/j.memsci.2016.01.033.
[15] C. Fonseka, S. Ryu, G. Naidu, J. Kandasamy, S. Vigneswaran, Recovery of water and valuable metals using low pressure nanofiltration and sequential adsorption from acid mine drainage, Environ. Technol. Innov. (2022), 102753, https://doi.org/10.1016/j.eti.2022.102753.
[16] S. Santoro, H. Estay, A.H. Avci, L. Pugliese, S. Straface, E. Curcio, Membrane technology for a sustainable copper mining industry: The Chilean paradigm, Clean. Eng. Technol. 2 (2021), 100091, https://doi.org/10.1016/j.clet.2021.100091.
[17] S. Al Obaidani, E. Curcio, G. Di Profio, E. Drioli, The role of membrane distillation/crystallization technologies in the integrated membrane system for seawater desalination, Desalin. Water Treat. 10 (2009) 210–219, https://doi.org/10.5004/dwt.2009.923.
[18] M. Ahmed, A. Arakel, D. Hoey, M.R. Thumarukudy, M.F.A. Goosen, M. Al-Haddabi, A. Al-Belushi, Feasibility of salt production from inland RO desalination plant reject brine: A case study, Desalination 158 (2003) 109–117, https://doi.org/10.1016/S0011-9164(03)00441-7.
[19] B.A. Sharkh, A.A. Al-Amoudi, M. Farooque, C.M. Fellows, S. Ihm, S. Lee, S. Li, N. Voutchkov, Seawater desalination concentrate—a new frontier for sustainable mining of valuable minerals, Npj Clean Water. 5 (2022) 1–16, https://doi.org/10.1038/s41545-022-00153-6.
[20] D.G. Randall, J. Nathoo, A succinct review of the treatment of Reverse Osmosis brines using Freeze Crystallization, J. Water Process Eng. 8 (2015) 186–194, https://doi.org/10.1016/j.jwpe.2015.10.005.
[21] Y. Tanaka, R. Ehara, S. Itoi, T. Goto, Ion-exchange membrane electrodialytic salt production using brine discharged from a reverse osmosis seawater desalination plant, J. Memb. Sci. 222 (2003) 71–86, https://doi.org/10.1016/S0376-7388(03)00217-5.
[22] L.N. Nthunya, M.F. Bopape, O.T. Mahlangu, B.B. Mamba, B. Van der Bruggen, C. A. Quist-Jensen, H. Richards, Fouling, performance and cost analysis of membrane-based water desalination technologies: A critical review, J. Environ. Manage. 301 (2022), 113922, https://doi.org/10.1016/j.jenvman.2021.113922.
[23] O.T. Mahlangu, L.N. Nthunya, M.M. Motsa, E. Morifi, H. Richards, B.B. Mamba, Fouling of high pressure-driven NF and RO membranes in desalination processes: Mechanisms and implications on salt rejection, Chem. Eng. Res. Des. 199 (2023) 268–295, https://doi.org/10.1016/j.cherd.2023.09.037.
[24] E. Drioli, G. Di Profio, E. Curcio, Progress in membrane crystallization, Curr. Opin. Chem. Eng. 1 (2012) 178–182, https://doi.org/10.1016/j.coche.2012.03.005.
[25] A. Ali, C.A. Quist-Jensen, F. Macedonio, E. Drioli, Application of membrane crystallization for minerals’ recovery from produced water, Membranes 5 (2015) 772–792, https://doi.org/10.3390/membranes5040772.

[26] P. Das, S. Dutta, K. Kumar, Insights into membrane crystallization: A sustainable tool for value added product recovery from effluent streams, Sep. Purif. Technol. 257 (2021), 117666, https://doi.org/10.1016/j.seppur.2020.117666.
[27] I. Chimanlal, L.N. Nthunya, C. Quist-Jensen, H. Richards, Membrane distillation crystallization for water and mineral recovery: The occurrence of fouling and its control during wastewater treatment, Front. Chem. Eng. 4 (2022) 1–14, https://doi.org/10.3389/fceng.2022.1066027.
[28] M. Qu, S. You, L. Wang, Insights into nucleation and growth kinetics in seeded vacuum membrane distillation crystallization, J. Memb. Sci. 620 (2021), 118813, https://doi.org/10.1016/j.memsci.2020.118813.
[29] B.K. Pramanik, K. Thangavadivel, L. Shu, V. Jegatheesan, A critical review of membrane crystallization for the purification of water and recovery of minerals, Rev. Environ. Sci. Biotechnol. 15 (2016) 411–439, https://doi.org/10.1007/s11157-016-9403-0.
[30] Y. Choi, G. Naidu, L.D. Nghiem, S. Lee, S. Vigneswaran, Membrane distillation crystallization for brine mining and zero liquid discharge: Opportunities, challenges, and recent progress, Environ. Sci. Water Res. Technol. 5 (2019) 1202–1221, https://doi.org/10.1039/c9ew00157c.
[31] I. Chimanlal, L.N. Nthunya, C. Quist-Jensen, H. Richards, Resource recovery from acid mine drainage in membrane distillation crystallization, Front. Membr. Sci. Technol. 2 (2023) 1–10, https://doi.org/10.3389/frmst.2023.1247276.
[32] Y. Zhou, L. Chen, M. Huang, W. Hu, G. Chen, B. Wu, Experimental investigation of the desalination process for direct contact membrane distillation using plate and frame membrane module, Appl. Sci. 13 (2023) 9439, https://doi.org/10.3390/app13169439.
[33] A.H.M. Zaheer, L. Gzara, A. Iqbal, F. Macedonio, M. Albeirutty, E. Drioli, Exergetic analysis of direct contact membrane distillation (DCMD) using PVDF hollow fiber membranes for the desalination brine treatment, Heliyon 9 (2023), https://doi.org/10.1016/j.heliyon.2023.e20927.
[34] V. Spillar, D. Dolejs, Calculation of Time-dependent Nucleation and Growth Rates from Quantitative T extural Data: Inversion of Crystal Size Distribution, J. Petrol. 54 (2013) 913–931, https://doi.org/10.1093/petrology/egs091.
[35] M. Gryta, Effectiveness of water desalination by membrane distillation process, Membranes 2 (2012) 415–429, https://doi.org/10.3390/membranes2030415.
[36] J. Gu, Y. Wu, G. Tang, Q. Wang, J. Lyu, Experimental study of heat transfer and bubble behaviors of NaCl solutions during nucleate flow boiling, Exp. Therm. Fluid Sci. 109 (2019), 109907, https://doi.org/10.1016/j.expthermflusci.2019.109907.
[37] L. Eykens, K. De Sitter, C. Dotremont, W. De Schepper, L. Pinoy, B. Van Der Bruggen, Wetting resistance of commercial membrane distillation membranes in waste streams containing surfactants and oil, Appl. Sci. 7 (2017) 118, https://doi.org/10.3390/app7020118.
[38] T.J. Mpala, H. Richards, A. Etale, O.T. Mahlangu, L.N. Nthunya, Carbon nanotubes and silver nanoparticles modification of PVDF membranes for improved seawater desalination in direct contact membrane distillation, Front. Membr. Sci. Technol. 2 (2023) 1–11, https://doi.org/10.3389/frmst.2023.1165678.
[39] F. Jiménez-Ángeles, A. Firoozabadi, Hydrophobic hydration and the effect of NaCl salt in the adsorption of hydrocarbons and surfactants on clathrate hydrates, ACS Cent. Sci. 4 (2018) 820–831, https://doi.org/10.1021/acscentsci.8b00076.
[40] O.R. Lokare, P. Ji, S. Wadekar, G. Dutt, R.D. Vidic, Concentration polarization in membrane distillation: I. Development of a laser-based spectrophotometric method for in-situ characterization, J. Memb. Sci. 581 (2019) 462–471, https://doi.org/10.1016/j.memsci.2019.03.080.
[41] W. Ni, Y. Li, J. Zhao, G. Zhang, X. Du, Y. Dong, Simulation study on direct contact membrane distillation modules for high-concentration nacl solution, Membranes 10 (2020) 1–18, https://doi.org/10.3390/membranes10080179.
[42] N.A. Mohammad Ameen, S.S. Ibrahim, Q.F. Alsalhy, A. Figoli, Highly salinewater desalination using direct contact membrane distillation (DCMD): Experimental and simulation study, Water 12 (2020) 1–24, https://doi.org/10.3390/W12061575.
[43] N.A. Ahmad, P.S. Goh, L.T. Yogarathinam, A.K. Zulhairun, A.F. Ismail, Current advances in membrane technologies for produced water desalination, Desalination 493 (2020), 114643, https://doi.org/10.1016/j.desal.2020.114643.
[44] M.T. Chan, A.G. Fane, J.T. Matheickal, R. Sheikholeslami, Membrane distillation crystallization of concentrated salts - Flux and crystal formation, J. Memb. Sci. 257 (2005) 144–155, https://doi.org/10.1016/j.memsci.2004.09.051.
[45] M.L. García-Lorenzo, J. Marimón, M.C. Navarro-Hervás, C. Pérez-Sirvent, M. J. Martínez-Sánchez, J. Molina-Ruiz, Impact of acid mine drainages on surficial waters of an abandoned mining site, Environ. Sci. Pollut. Res. 23 (2016) 6014–6023, https://doi.org/10.1007/s11356-015-5337-2.
[46] C.M. Tun, A.G. Fane, J.T. Matheickal, R. Sheikholeslami, Membrane distillation crystallization of concentrated salts—flux and crystal formation, J. Memb. Sci. 257 (2005) 144–155, https://doi.org/10.1016/j.memsci.2004.09.051.
[47] N.T.K. Thanh, N. Maclean, S. Mahiddine, Mechanisms of nucleation and growth of nanoparticles in solution, Chem. Rev. 114 (2014) 7610–7630, https://doi.org/10.1021/cr400544s.
[48] J.W. Mullin, Crystallization, 4th ed., Elsevier, 2001.
[49] M.R.N. Soares, S. Leite, C. Nico, M. Peres, A.J.S. Fernandes, M.P.F. Graça, M. Matos, R. Monteiro, T. Monteiro, F.M. Costa, Effect of processing method on physical properties of Nb2O5, J. Eur. Ceram. Soc. 31 (2011) 501–506, https://doi.org/10.1016/j.jeurceramsoc.2010.10.024.
[50] B.Y. Shekunov, P. Chattopadhyay, H.H.Y. Tong, A.H.L. Chow, Particle size analysis in pharmaceutics: Principles, methods and applications, Pharm. Res. 24 (2007) 203–227, https://doi.org/10.1007/s11095-006-9146-7.
[51] I.A. Mudunkotuwa, T. Rupasinghe, C.M. Wu, V.H. Grassian, Dissolution of ZnO nanoparticles at circumneutral pH: A study of size effects in the presence and absence of citric acid, Langmuir 28 (2012) 396–403, https://doi.org/10.1021/la203542x.
[52] J. Liu, D.M. Aruguete, J.R. Jinschek, J. Donald Rimstidt, M.F. Hochella, The non-oxidative dissolution of galena nanocrystals: Insights into mineral dissolution rates as a function of grain size, shape, and aggregation state, Geochim. Cosmochim. Acta. 72 (2008) 5984–5996, https://doi.org/10.1016/j.gca.2008.10.010.
[53] L. Dang, H. Wei, Z. Zhu, J. Wang, The influence of impurities on phosphoric acid hemihydrate crystallization, J. Cryst. Growth 307 (2007) 104–111, https://doi.org/10.1016/j.jcrysgro.2007.05.041.